

# Discovery of Small Molecule CD40–TRAF6 Inhibitors

Barbara Zarzycka,<sup>†</sup> Tom Seijkens,<sup>‡</sup> Sander B. Nabuurs,<sup>§,||</sup> Tina Ritschel,<sup>||</sup> Jochen Grommes,<sup>⊥</sup> Oliver Soehnlein,<sup>#</sup> Roy Schrijver,<sup>†</sup> Claudia M. van Tiel,<sup>‡</sup> Tilman M. Hackeng,<sup>†</sup> Christian Weber,<sup>#</sup> Fabian Giehler,<sup>▽</sup> Arnd Kieser,<sup>▽</sup> Esther Lutgens,<sup>‡,#</sup> Gert Vriend,<sup>||</sup> and Gerry A. F. Nicolaes<sup>\*,†</sup>

<sup>†</sup>Department of Biochemistry, Cardiovascular Research Institute Maastricht (CARIM), Maastricht University, 6200 MD Maastricht, The Netherlands

<sup>‡</sup>Department of Medical Biochemistry, Subdivision of Experimental Vascular Biology, Academic Medical Center, University of Amsterdam, 1105 AZ Amsterdam, The Netherlands

<sup>§</sup>Lead Pharma Medicine, 5349 AC Oss, The Netherlands

<sup>||</sup>CMBI, Radboud University Medical Centre, P.O. Box 9101, 6500 HB Nijmegen, The Netherlands

<sup>⊥</sup>European Vascular Center Aachen-Maastricht, RWTH Aachen, 52062 Aachen, Germany

<sup>#</sup>Institute for Cardiovascular Prevention, Ludwig Maximilians University, 80336 Munich, Germany

<sup>▽</sup>Research Unit Gene Vectors, Helmholtz Zentrum München – German Research Center for Environmental Health, 81377 Munich, Germany

## S Supporting Information

**ABSTRACT:** The CD154–CD40 receptor complex plays a pivotal role in several inflammatory pathways. Attempts to inhibit the formation of this complex have resulted in systemic side effects. Downstream inhibition of the CD40 signaling pathway therefore seems a better way to ameliorate inflammatory disease. To relay a signal, the CD40 receptor recruits adapter proteins called tumor necrosis factor receptor-associated factors (TRAFs). CD40–TRAF6 interactions are known to play an essential role in several inflammatory diseases. We used *in silico*, *in vitro*, and *in vivo* experiments to identify and characterize compounds that block CD40–TRAF6 interactions. We present in detail our drug docking and optimization pipeline and show how we used it to find lead compounds that reduce inflammation in models of peritonitis and sepsis. These compounds appear to be good leads for drug development, given the observed absence of side effects and their demonstrated efficacy for peritonitis and sepsis in mouse models.



## ■ INTRODUCTION

CD40 is a transmembrane protein receptor that belongs to the tumor necrosis factor (TNF) receptor superfamily and is primarily present on antigen-presenting cells. It can be activated by its ligand CD154 (also known as CD40L or GP39), which is a transmembrane glycoprotein. CD154 is transiently expressed on activated T cells and other nonimmune cells under inflammatory conditions, and is also found in a soluble form. Binding results in CD40 homotrimerization and intracellular recruitment of TNF receptor-associated factors (TRAFs) that subsequently elicit signaling.<sup>1</sup> CD40 can bind TRAF 1, 2, 3, 5, and 6. Two different binding sites have been determined in the intracellular domain of CD40: one for TRAF 2, 3, and 5 and one for TRAF6.<sup>2</sup> The 180 amino acid long C-domain of the TRAF family proteins can bind to the cytosolic domain of CD40.<sup>3</sup> CD40 signaling can activate downstream pathways such as the NF- $\kappa$ B, C-Jun N-terminal kinase (JNK), or the p38 mitogen-activated protein (MAP) kinase pathway, depending on which TRAFs gets recruited.<sup>2</sup> CD154–CD40 interactions play a pivotal role in immunity by, for example, promoting T cell activation and immunoglobulin isotype switching.<sup>1</sup> Moreover, the CD154–CD40 complex is involved in the patho-

genesis of (chronic) inflammatory diseases<sup>4</sup> like atherosclerosis, inflammatory bowel disease, psoriasis, systemic lupus erythematosus, rheumatoid arthritis, allograft rejection, and obesity-associated inflammation and insulin resistance. The CD154–CD40 complex has been shown to be a good target for drug design projects, and antibodies for CD154 and CD40 have reached phase I and phase II clinical trials in the development of drug treatments for multiple sclerosis, psoriasis,<sup>5</sup> lupus nephritis,<sup>6</sup> and systemic lupus erythematosus.<sup>7</sup> Long-term inhibition of CD154–CD40 interactions by small molecule ligands<sup>8</sup> or monoclonal antibodies<sup>9</sup> is not clinically feasible because of envisioned immune suppression or, for CD154, thrombo-embolic complications.<sup>9</sup> More downstream inhibition of the CD40 signaling pathway therefore seems a better approach.

We have shown that interaction of CD40 with TRAF6 (but not with TRAF 2, 3, and 5) is involved in the development of atherosclerosis<sup>10</sup> and obesity-associated insulin resistance.<sup>11</sup> These interactions occur downstream from CD40, making

Received: October 20, 2014

Published: January 27, 2015

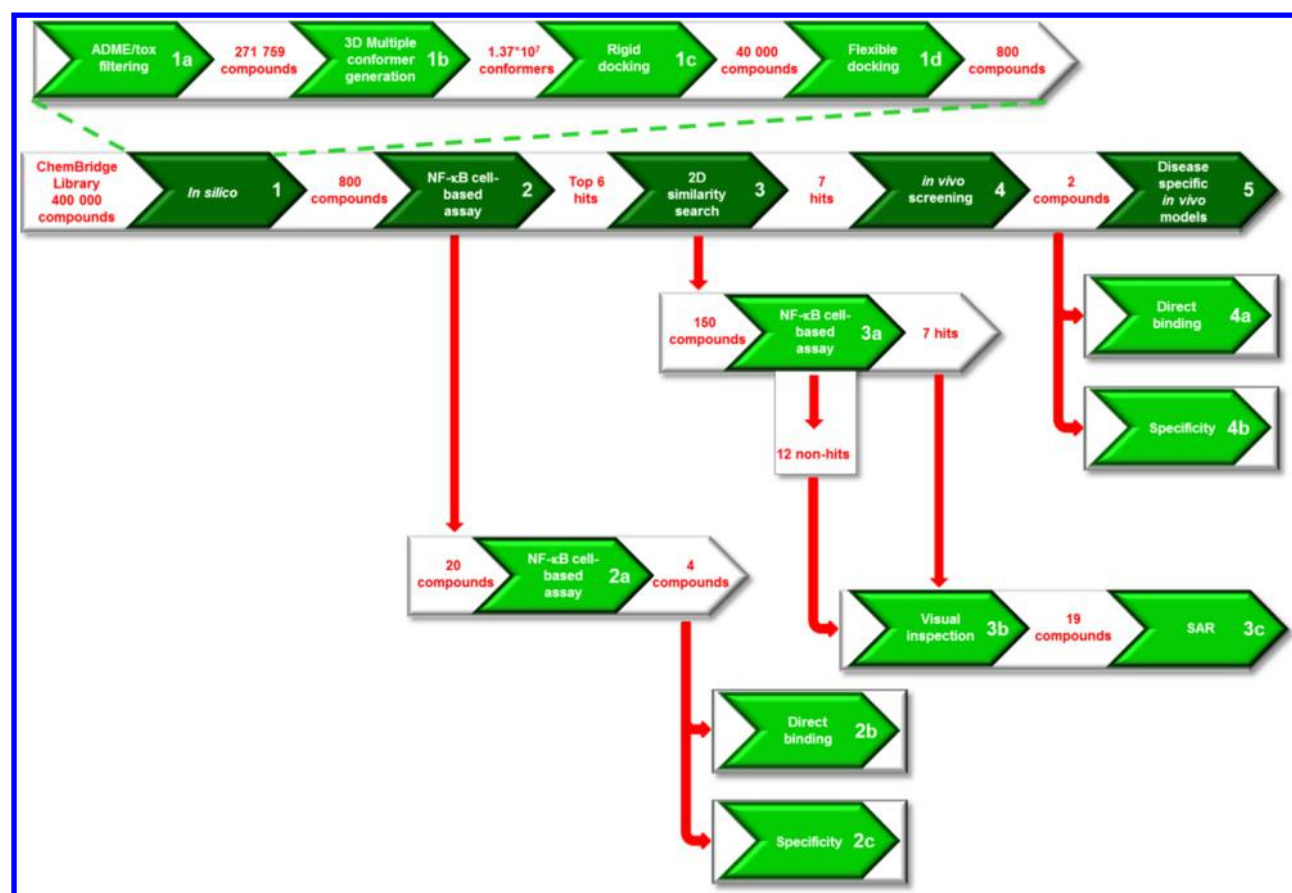


**Figure 1.** Schematic of the drug selection pipeline, illustrating the step-by-step the process of extracting a small subset of candidate lead compounds from the ChemBridge library of 400,000 compounds. The main pathway in dark green consists of (1) *in silico* reduction of the data set, (2) *in vitro* cell-based assay, (3) *in silico* similarity searches, (4) *in vivo* screening (peritonitis model), and (5) *in vivo* disease-specific (sepsis, insulin resistance, arteriosclerosis, multiple sclerosis) tests. In step 1, the *in silico* data reduction consists of (1a) ADME/tox filtering, (1b) 3D conformer generation, (1c) rigid docking, and (1d) flexible docking. The additional steps in the pipeline (direct binding studies, visual inspection, specificity measurements, and SAR, depicted in 2ab, 3bc, and 4ab) all are aimed at ligand optimization and at a better understanding of how the ligand binds.

them a better entry point for pharmacological intervention because some of the other functions of CD40 signaling would remain intact, presumably limiting immunosuppressive side effects.<sup>10</sup> One of the compounds that functionally blocks CD40–TRAF6 signaling is a potent (and safe) inhibitor in obesity-associated insulin resistance in mouse models.<sup>11</sup> Here, we present comprehensive details of the drug selection pipeline and extend it by inclusion of two additional ligand optimization strategies that resulted in new compounds with different scaffolds. We also show that the compounds are active, ameliorating peritonitis and sepsis in addition to diet-induced obesity.

## MATERIALS AND METHODS

**Protein Target Preparation.** The X-ray structure of the TRAF6 C-domain in complex with a CD40 fragment (PDB ID: 1LB6; resolution 1.80 Å<sup>12</sup>) and the TRAF6 C-domain apo structure (PDB ID: 1LB4; resolution 2.40 Å<sup>12</sup>) were retrieved from the Protein Databank (PDB<sup>13</sup>), as described before.<sup>11</sup> The YASARA-WHAT IF Twinset package<sup>14</sup> was used to add hydrogen atoms and optimize their positions. This optimization includes the WHAT IF<sup>15</sup> procedure that predicts His, Glu, and Asp ionization states (all of which were normal) and side chain flips of His, Asn, and Gln (three Gln, five His, and one Asn side chains were flipped). The co-crystallized CD40 fragment was

removed before hydrogen optimization, and all solvent molecules were removed afterward. During structure optimization the YASARA-WHAT IF Twinset additionally removes atomic clashes with an unrestrained steepest descent energy minimization, and normalizes extreme bond lengths and angles.

X-ray structures were superposed with the MOTIF algorithm<sup>16</sup> as implemented in the YASARA-WHAT IF Twinset package.

Arg466 is missing in the apo structure (PDB ID: 1LB4) suggesting that this residue is very flexible. Arg466 is involved in interactions with the CD40 peptide fragment, which causes it to be located inside the druggable pocket in the holo structure (PDB ID: 1LB6). We used YASARA's backbone dependent rotamer library<sup>17</sup> to guide the manual placement of Arg466 outside this pocket.

ICM PocketFinder<sup>18</sup> and Q-SiteFinder<sup>19</sup> were used to detect druggable pockets. ICM PocketFinder explores possible binding pockets using an algorithm based on a transformation of the Lennard–Jones potential. The Q-SiteFinder program uses interaction energies between the protein and a van der Waals probe to determine favorable binding sites. Both programs were used with default settings for all parameters.

**Ligand Database Preparation.** The drug selection pipeline depicted in Figure 1 starts with an *in silico* small molecule collection that was retrieved from the Express Pick ChemBridge database<sup>20</sup> (June 2010 version). This version of

the library contained 400,000 well-described and commercially available compounds.

The collection of small molecules was filtered (Figure 1, step 1a) using the FAF-Drugs2<sup>21</sup> (version June 2010) ADME/tox (administration, delivery, metabolism, extraction, and toxicity) filter that eliminates nondrug-like molecules using a Lipinski rule-of-five filter (molecular weight  $\leq 500$ , cLogP  $\leq 5$ , number of H-bond donors  $\leq 5$ , number of acceptors  $\leq 10$ , and number of rotatable bonds  $\leq 5$ ), while accepting molecules that maximally violate one of these rules. Additionally, compounds containing reactive groups (e.g., nitro derivatives) or toxic groups (e.g., aniline)<sup>22</sup> were rejected. Salts and counterions were removed from the small molecule files with the DeSalt utility of the FAF-Drugs2 program.<sup>23</sup>

The OMEGA software (OpenEye, v 2.1.0<sup>24</sup>) was used in step 1b in Figure 1 to generate 3D multiconformers. OMEGA was also used to add hydrogen atoms and Gasteiger partial charges to the ligands. OMEGA uses a modified version of the MMFF94s force field with omitted Coulomb terms. Defaults were used for all parameters including the ewindow value that determines the strain energy range, and the root-mean-square deviation (RMSD) parameter that determines minimally required conformer similarity. The maximum number of conformers per compound was 50.

**Virtual Ligand Screening (VLS).** The virtual ligand screening (VLS) pipeline consists of a multistep protocol<sup>11,25,26</sup>, including rigid-body docking, flexible docking, and 2D similarity searches.<sup>27,28</sup>

The first docking (Figure 1, step 1c) was performed with the rigid-body docking program FRED (fast rigid exhaustive docking) (v 2.2.5,<sup>27</sup>). FRED was used first because it is fast enough to dock more than 1,000,000 conformations in the multiconformer library that were generated by the OMEGA software. FRED generates one pose for each compound, independent of the number of conformers in the multiconformer. Resulting poses were ranked using FRED's consensus scoring function.<sup>27</sup> The 40,000 highest-ranked compounds were passed on to the next step in the pipeline, which employed Surflex-Dock (v 2.514<sup>29</sup>) for flexible docking. Surflex-Dock requires that an active site is predefined. We determined this active site by a consensus residue-based approach, using residues previously detected with ICM PocketFinder and Q-SiteFinder. Docking in Surflex-Dock was done with default parameters and the Surflex scoring function. For each compound, Surflex-Dock returns the best-scoring pose and its corresponding score. The 800 top-ranked compounds were purchased for *in vitro* screening.

**2D Similarity Searches.** Compound similarity searches were performed using the online search tool www.hit2lead.com<sup>28</sup> in the ChemBridge software suit. The top six compounds from the *in vitro* analyses were used as search queries to find analogues. Analogues were accepted when their Tanimoto coefficient<sup>30</sup> was greater than 0.8.

**Off-Target Prediction.** Off-target predictions were done with KRIPO (key representation of interaction in pockets).<sup>31</sup> KRIPO requires both the target protein and each protein in its search database to be available as a complex structure with a reference ligand that is presented in the PDB file as a heterogroup to define the binding site of the receptor. Thus cannot work with PDB files in which a bound peptide is presented as a macromolecule. Because we did not have an X-ray structure of compound 6877002 bound to TRAF6, we used the complex of TRAF6 with this compound docked as

described in the Virtual Ligand Screening (VLS) section (Table 2, compound 6), for the binding site determination. The features that represent possible interactions in the binding site (aromatic interactions, hydrogen bond acceptors and donors, hydrophobic contacts, and positive and negative charges) were converted into a pharmacophore. The pharmacophore was stored in a fingerprint format, which was used as a query to search for off-targets (modified Tanimoto coefficient, threshold 0.45<sup>31</sup>). For the off-target prediction, we used the March 2014 version of the KRIPO database of target–ligand complexes, which contained all protein–ligand complexes deposited in the PDB before April 2014.

**Binding Mode Prediction.** Docking calculations with inclusion of full ligand flexibility and side chain rotamer flexibility for a limited number of key residues were performed with Fleksy,<sup>32</sup> using default parameters. Fleksy requires a reference ligand to define the binding site of the receptor. As the reference ligand, we used the above-mentioned compound from the Surflex-Dock run (compound ID 6877002), the same as in the KRIPO search.

**Cell-Based Assay.** For the lipopolysaccharide (LPS)-induced NF- $\kappa$ B luciferase assay, the mouse monocyte/macrophage cell line (RAW 264.7) was stably transfected with the 3x- $\kappa$ Bluc plasmid.<sup>33</sup> Cells were incubated with compounds at 10  $\mu$ M for 1 h. Compounds were then tested individually in 96-well plates. CD40 expression was induced with LPS (10 ng/mL) from *E. coli* (Sigma-Aldrich). After 2 h, cells were lysed and incubated with a substrate containing luciferin according to the PNT9019D protocol by Applied Biosystems. Reaction with luciferin results in the emission of a light signal that is proportional to the amount of NF- $\kappa$ B signaling activation and that can be measured at 450 nm with a Wallac Victor II luminometer.

For CD40-induced macrophage activation, bone marrow (BM) cells were isolated from the femurs and tibias of C57BL/6 mice and cultured in RPMI with 15% L929-conditioned medium to generate BM-derived macrophages. The CD40 antibody (FGK45) was used (25  $\mu$ g/mL for 6 h) to activate BM-derived macrophages. Cells were incubated with 10  $\mu$ M compound for 1 h. Expression of IL1 $\beta$  and IL6 was analyzed using real-time PCR.

**Protein Expression and Purification.** The isolated C-domains of TRAF2 (residues 311–501), TRAF3 (residues 375–568), and TRAF6 (residues 310–522) were expressed and purified according to previously described methods.<sup>34,35</sup> The C-domain of TRAF1 (residues 226–416) were cloned via PCR (primer sequences are available on request) into a pET17 vector together with N-terminal His tag. Protein expression and purification were carried out as described for the other TRAFs. The intracellular part of CD40 (residues 216–277) was expressed in *E. coli*. The bacteria were lysed by sonication in phosphate-buffered saline with Triton X-100 (PBST) buffer. Cleared lysate was incubated for 4–6 h on 4 °C to bind to glutathione S-transferase (GST)-beads. Subsequently, the protein was washed three times with the PBST buffer and eluted with 10 mM Glutathione. Purification followed the previously described procedure for the other TRAFs.

**Direct Binding.** The C-domains of TRAF 1, 2, 3, and 6 were immobilized on a CM5 sensor chip using the amine-coupling method from GE Healthcare. The coupling reaction was continued until a total binding density of  $\sim 10200$ ,  $\sim 11500$ ,  $\sim 9800$ , and  $\sim 11200$  response units (RU) was achieved for TRAF1, TRAF2, TRAF3, and TRAF6, respectively. Com-



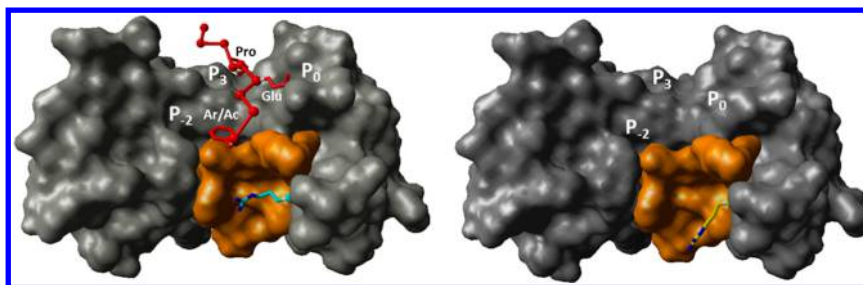


**Figure 2.** (a) Molecular surface of the TRAF6 C-domain (gray, PDB ID: 1LB6) in complex with a CD40 peptide fragment (red  $\alpha$ -trace). The residues of the Pro-X-Glu-X-(aromatic/acidic) motif that bind to the subpockets  $P_{-2}$  (Pro),  $P_0$  (Glu), and  $P_3$  (aromatic/acidic) are labeled.<sup>57</sup> The Arg466 side chain is shown colored by atom type. In panel (b), the Arg466 side chain has been manually moved as described in the text, opening up the druggable pocket that is colored orange.

pounds were dissolved in DMSO and diluted in phosphate-buffered saline (PBS) buffer (10 mM phosphate, pH 6.8) to a final concentration of 5% v/v DMSO, and final pH 7.4. Compounds were diluted into seven different concentrations. All experiments were done at 25 °C in surface plasmon resonance (SPR) with running buffer (PBS, 0.05% Tween 20, 5% (v/v) DMSO, pH 7.4) and a flow rate of 50  $\mu\text{L min}^{-1}$ . Binding curves were corrected by subtraction of the level of SPR signal observed on the empty reference flow channel during injection of the compounds. As a positive binding control, we used binding of the intracellular part of CD40 to the C-domains of TRAF 1, 2, 3, and 6. Equilibrium dissociation constants ( $K_{\text{d}}$ s) were determined with the steady-state affinity model<sup>36</sup> (average of at least two independent runs with seven different concentration for each compound) using the BIAevaluation software from GE Healthcare (v 1.0).

**Peritonitis.** To examine the influence of compounds on the acute inflammation response, we used an *in vivo* model of peritoneal inflammation. Inflammation was induced in male C57Bl6 mice ( $n = 6\text{--}8$  per compound) by intraperitoneal injection with 3 mL 4% sodium thioglycolate (Sigma) in PBS. Mice received intraperitoneal injection of compounds (10  $\mu\text{mol/kg}$ ) dissolved in vehicle (5% DMSO in PBS) 0, 6, 12, and 15 h after induction of inflammation. Injections with the vehicle only were used as a control. Euthanasia took place 18 h after induction of inflammation. Blood and peritoneal cells were collected. Leukocytes were analyzed according to the flow cytometry protocol described below.

**Flow Cytometry.** To determine the effect of compounds on the acute inflammation response we analyzed blood cells. At the time of sacrifice, blood was obtained from the heart using EDTA-coated syringes. Erythrocytes were lysed by addition of a hypotonic buffer (8.4 g of  $\text{NH}_4\text{Cl}$  and 0.84 g of  $\text{NaHCO}_3$  per liter of distilled water). Nonspecific antibody binding was prevented by preincubation with a Fc-receptor blocking antibody (eBioscience). Leukocytes were labeled with CD3-FITC (eBioscience), B220-V500 (eBioscience), CD11b-PeCy7 (BD), Ly6G-PE (BD), and Ly6C-APC (Miltenyi Biotec). Cells were analyzed on a FACS Canto II flow cytometer (BD).

**Toxicity.** Cytotoxicity of compounds was tested on RAW 264.7 cells incubated with 10  $\mu\text{M}$  compounds for 1 h, followed by analysis using a Casy cell counter according to the manufacturer's protocol (Roche Applied Science). *In vivo* toxicity was tested on male C57Bl6 mice with peritoneal inflammation. Mice received intraperitoneal injection of compounds (10  $\mu\text{mol/kg}$ ) for seven days, as described in aforementioned Peritonitis section. The absolute peripheral

blood leukocyte counts were analyzed using a scil Vet ABC Plus hematology analyzer (Scil Animal Care Company B.V.). Thirteen organs were prepared in paraformaldehyde (4%, overnight), sectioned at 4  $\mu\text{m}$ , and stained with eosin and hematoxylin for histological studies.

**Sepsis.** Sepsis was induced by cecal ligation and puncture (CLP).<sup>37</sup> Mice were anesthetized with an intraperitoneal injection of ketamine (125 mg/kg body weight; Sanofi-Ceva GmbH Düsseldorf, Germany) and xylazine (12.5 mg/kg body weight; Phoenix Scientific). The abdomen was opened by longitudinal midline incision, and then the cecum was filled with feces, ligated 1 cm behind the tip, and punctured with a 22 gauge needle, followed by the pressing out of a small amount of feces. Fascia, abdominal musculature, and skin were closed by running sutures. Sham mice underwent the same surgical procedure without inducing sepsis (i.e., placebo surgery). Mice were treated with either compound 6877002 or 6860766 (10  $\mu\text{mol/kg}$ ) or with just the vehicle during CLP and 12 h after CLP via intraperitoneal injection.

**Study Approval.** All animal experiments were approved by the local Animal Experimentation Committees.

## RESULTS

**Protein Target Preparation.** Many small differences were observed between the TRAF6 apo and holo structures that could be interpreted as conformational changes resulting from binding of the CD40 peptide. We decided to use the holo structure comprising the TRAF6 C-domain structure after CD40 peptide deletion for VLS, because in this structure, the conformations of amino acid side chains in the pocket corresponds to those of the ligand bound state of the TRAF6 C-domain, which minimizes the chance that major pocket changes are still needed to accommodate a ligand.<sup>38</sup>

Pro465, Arg466, Asn467, and Pro468, located in a loop that lines the peptide-binding groove, are not present in the X-ray structure of the apo TRAF6 C-domain, presumably because mobility or disorder precluded them from being seen in the electron density maps. On the other hand, these same residues are present in the CD40-TRAF6 C-domain complex structure. The absence of these residues in the apo structure strengthens the observation that the conformation of these residues in the holo structure is the result of interactions with the short CD40 peptide. In the holo structure, Arg466 is located in the peptide binding groove in an area where full-length CD40 presumably binds (Figure 2a) but which is unbound in the apo structure. We therefore chose to select a side chain conformation for Arg466 such that the chosen rotamer leaves the pocket as widely open as possible (Figure 2b).

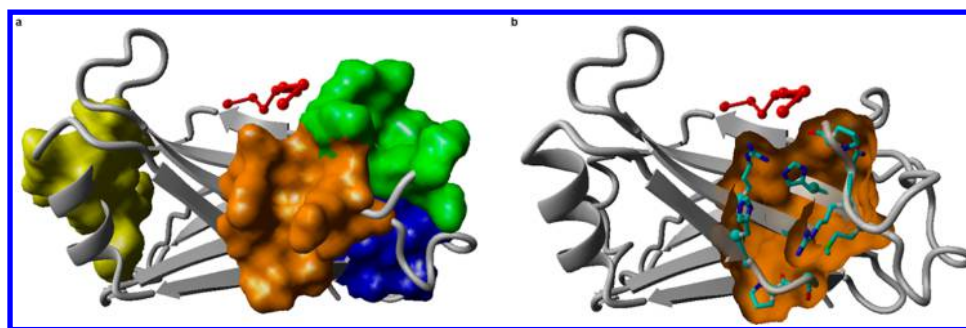


**Figure 3.** Predicted druggable pockets. (a) ICM PocketFinder: four druggable pockets were predicted with the following volumes and areas: 158 Å<sup>3</sup> and 177 Å<sup>2</sup> (orange), 127 Å<sup>3</sup> and 140 Å<sup>2</sup> (green), 104 Å<sup>3</sup> and 116 Å<sup>2</sup> (blue), and 163 Å<sup>3</sup> and 218 Å<sup>2</sup> (yellow). (b) The selected pocket (orange) is surrounded by the following amino acid residues: His376, Pro378, Gly379, Cys390, Arg392, His412, Met414, Arg466, Asn467, and Pro468.

**Table 1.** Structures of Six Initial Hits Obtained after *in silico* Steps 1a–d and Luciferase NF-κB Cell-Based Assay

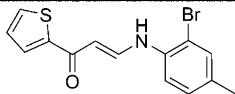
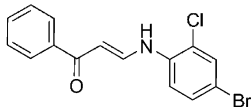
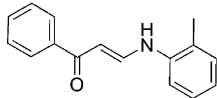
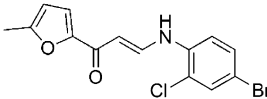
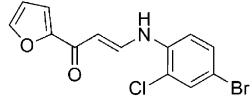
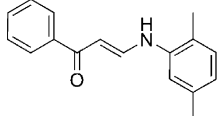
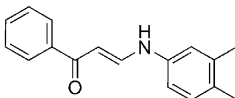
Compound #	ChemBridge ID	MW (kDa)	Structure
1	7002991	360	
2	7148854	363	
3	7170791	324	
4	6877002	251.3	
5	9049194	255	
6	9053705	258	

ICM PocketFinder predicted four druggable pockets in the receptor model<sup>11</sup> (Figure 3a). The pocket that we selected for targeting has a volume of 158 Å<sup>3</sup> (Figure 3b). This pocket was selected because it has one of the largest predicted pocket volumes. Q-SiteFinder detected several druggable pockets. The pocket located closest to the peptide groove has a volume of 139 Å<sup>3</sup> and was approximately in the same location as the largest pocket predicted by the ICM PocketFinder. Thus, the pocket that was chosen for the VLS was the consensus from the

best pockets predicted by both programs. Moreover, this pocket appears to be part of what can be seen as an extended binding groove along the central axis of the molecule to which the CD40 peptide is also bound (Figures 2a and 3a). We hypothesized that binding of small molecules to this pocket could therefore interfere with CD40–TRAF6 interaction.

**Ligand Selection.** Our *in silico* drug selection pipeline consisted of a Lipinski filter, quick and dirty rigid docking, intermediately precise flexible docking, and exhaustive docking

Table 2. Structures and IC<sub>50</sub> Values ( $\mu$ M) of “Seven Hits” from NF- $\kappa$ B Assay

Compound #	ChemBridge ID	MW (kDa)	IC <sub>50</sub> ( $\mu$ M)	Structure
1	7805351	322.2	0.1	
2	6860766	336.6	0.3	
3	6876358	237.3	1.5	
4	7493979	340.6	3.2	
5	7651589	326.6	3.5	
6	6877002	251.3	16	
7	6872674	251.3	16	

with inclusion of side-chain rotamer flexibility. The full pipeline also included *in vitro* and *in vivo* validation steps. We previously used this pipeline to find a ligand that showed efficacy in a diet-induced insulin-resistant mouse model.<sup>11</sup> Here, we extend this pipeline with steps aimed at selecting more ligands and steps aimed at optimization of the ligand structures. Figure 1 illustrates the extended pipeline. The results of steps 1a–d were described before<sup>11</sup> and will not be repeated here.

The 800 best docking compounds were purchased from ChemBridge (www.chembridge.com) for *in vitro* testing (Figure 1, step 2). The number 800 was a compromise between the price of compounds and labor costs of *in vitro* testing on the one hand and on the other hand the desire to obtain a considerable number of hits (in previous drug design projects, we often experienced hit rates around 1–2%<sup>39,40</sup>). Similar financial constraints restricted the number of compounds in all following steps (Figure 1, step 2).

The top six compounds from the initial *in vitro* screen that are listed in Table 1 show some similarities. All six compounds share a linker that is three to six atoms long, that contain N and O atoms, and that connects two, often substituted, six-membered rings. The docking poses are presented in Figure 1 of the Supporting Information. The six compounds were used as a search query for a 2D similarity search that led to 151 new compounds. These 151 compounds were tested using the cell-based luciferase NF- $\kappa$ B assay. Eight of the 151 compounds inhibited NF- $\kappa$ B signaling by more than 25% at 10  $\mu$ M, and six

of these eight compounds showed dose-dependent behavior. These six best compounds were analogues of compound 6877002, and together with the single query compound that was used to retrieve them in the 2D similarity search, all of them showed inhibition with IC<sub>50</sub> values in the low  $\mu$ M range. These seven compounds are referred to as the “seven hits” and are summarized in Table 2.

The seven compounds listed in Table 2 are less diverse than the six compounds identified in the primary screening in that they all share an identical four-atom long linker containing a Michael acceptor functionality and an N–H group. This linker connects two five- or six-atom rings that are often ortho- or para-substituted with the small groups CH<sub>3</sub>, Br, or Cl. When we inspected the nonbinders and poor binders among the 151 compounds that resulted from the 2D similarity search, we detected 12 additional compounds with exactly the same linker and highly similar five- or six-atom substituted rings. These 12 compounds (Table 3) have in common that one of the two rings is meta-substituted, hinting at a possible understanding of the structure–activity relationship for these small molecules. All 12 have an IC<sub>50</sub> higher than the detection limit of 100  $\mu$ M.

**Biological Evaluation.** Pro-inflammatory cytokines play a pivotal role in the inflammatory response. We used primary BM-derived macrophages and stimulated them with the CD40 agonist FGK45<sup>11</sup> to determine the change in mRNA expression of IL6 and IL1 $\beta$  upon incubation with the seven best compounds shown in Table 2. It was only used for the seven

Table 3. Compounds Similar to Seven Hits That Have an  $IC_{50}$  Higher than Detection Limit of 100  $\mu M$ 

Compound #	ChemBridge ID	MW (kDa)	Structure
1	6613327	265.4	
2	5929451	223.3	
3	5404871	271.7	
4	7235862	269.3	
5	7645440	261.7	
6	5404859	285.8	
7	5404895	350.6	
8	6873719	301.8	
9	6875452	306.2	
10	6876201	330.2	
11	6876350	281.4	
12	6876773	285.8	

best hits because it is more laborious and much more expensive than the LPS-induced NF- $\kappa$ B assay used for the primary screen. All seven hits inhibited the expression of IL1 $\beta$  and IL6 cytokines in primary BM-derived macrophages in a dose-dependent manner with  $IC_{50}$ s in the range 0.2 to >100  $\mu M$  (Table 4).

Table 4.  $IC_{50}$  Values ( $\mu M$ ) of Seven Hits That Inhibited CD40-Induced Expression of IL1 $\beta$  and IL6 in Bone Marrow-Derived Macrophages

compound	compound ID	IL1 $\beta$ , $IC_{50}$ ( $\mu M$ ) <sup>b</sup>	IL6, $IC_{50}$ ( $\mu M$ ) <sup>b</sup>
1	7805351 <sup>a</sup>	>100	>100
2	6860766	5.7	2.4
3	6876358	24	21
4	7493979	4.6	2.2
5	7651589	1.9	0.3
6	6877002	16	50
7	6872674	1.4	0.2

<sup>a</sup>Activity of compound 7805351 was above 100  $\mu M$  in this assay, however in the NF- $\kappa$ B assay (Table 2), it had the best  $IC_{50}$  with value of 0.1  $\mu M$ . Thus, we consider it as a good binder. <sup>b</sup>The errors in the  $IC_{50}$  values might be up to factor of 2 because of biological variability between the experiments such as variation in the time of initiation of transcription of IL1 $\beta$  and IL6 after FGK45 binding, variation in medium composition among the experiments, variation in the differentiation of the bone marrow-derived macrophages and their metabolic and inflammatory state, and many other natural differences between the mice from which the bone marrow was harvested.

The primary data used for the calculation of  $IC_{50}$  values presented in Table 4 are shown in Figure 2 of the Supporting Information.

**Binding Mode of Inhibitors.** The seven hits that were characterized with the two cell-based assays (Figure 1) and their 12 inactive analogues were docked on the TRAF6 target structure with Flexy.<sup>32</sup> Flexy requires a reference compound to define the binding site. We used the coordinates of compound 6877002 docked with Surflex-Dock. Flexy produced 20 poses for each compound and calculated a consensus score.<sup>41</sup> We manually compared all 380 poses, looking for common protein–ligand interaction motifs. For eight compounds, we found a common binding mode that includes hydrogen bonds with residues Asn467 and Cys390 and  $\pi$ – $\pi$  stacking of Arg466 and His376 on the ligand's R1 ring (Figure 4). The seven good inhibitory compounds were among these eight. Six of the other 12 compounds did not include a hydrogen bond with Asn467, while five of the 12 did not resemble the common binding mode at all.

As previously described,<sup>11</sup> the 19 compounds all have a similar topology. They possess the same linker that connects two similar rings. We hypothesized that all active compounds will bind in a similar manner, and we assumed that the inactive compounds are inactive because they cannot adopt that same binding mode. To validate this idea, all compounds were exhaustively docked with Flexy, with the additional constraint that their common cores had to align to the common core of the active compound 7805351. This compound is one of the seven good inhibitors among the 19 in the NF- $\kappa$ B assay (Table 2). The docking poses obtained in this manner looked plausible except for one interatomic clash between the groups at the meta position of the R1 ring of the ligand and Pro468. Indeed, good activity of the compounds appears to correlate with the absence of meta substituents and to a lesser extent also with the presence of substituents at either the ortho or para position. Compound 5929451 does not have substituents at either the R1 or the R2 ring. This compound has an  $IC_{50}$  value above 100  $\mu M$ , suggesting that substituents at the R1 ring are crucial to obtaining low  $IC_{50}$  values.

**Structure–Activity Relationship (SAR).** To unravel the structure–activity relationship (SAR) of the inhibitors of



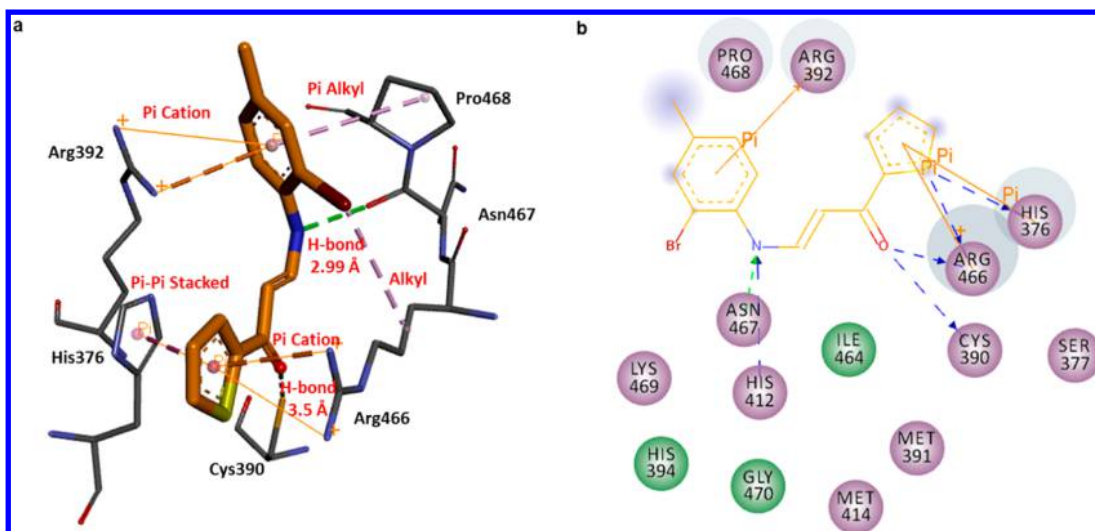


**Figure 4.** Docking pose of compound 7805351. (a) The 7805351 interactions with TRAF6 protein in a 3D representation. (b) 2D representation, polar (magenta circles), van der Waals (green circles), H-bond with acid side chain (blue arrow), H-bond with acid main chain (green arrow),  $\pi$ - $\pi$  interactions (orange lines), and  $\pi$  alkyl and  $\pi$  cation interactions (purple dashed lines).

**Table 5. Structures and  $IC_{50}$  Values ( $\mu M$ ) of Compound 7805351 Analogues**

Compound #	ID	MW (kDa)	$IC_{50}$ ( $\mu M$ )	Structure
1	F6176-1890	298.2	20	
2	F6176-1927	289.4	48	
3	F6176-1970	259.3	21	

CD40–TRAF6 interaction, an additional set of 25 compounds was synthesized.<sup>42</sup> These are analogues of compound 7805351 with different substitution groups present only at the R1 ring. We proposed 10 compounds based on the ligand analysis and 12 compounds based on the structure analysis of the previously proposed binding mode. Three compounds with very big substitution groups in both the ortho and para positions were chosen as proposed negative controls of our binding mode hypothesis. Out of these 25 compounds, only three compounds were weakly active and had  $IC_{50}$  values in the NF- $\kappa B$  cell-based assay that were lower than 100  $\mu M$  (Table 5). These three compounds have substitution groups present at both the para and the ortho position. Compounds with substituents at only the ortho or only the para position were inactive. Compounds with very small, very big, or charged substitution groups in these crucial positions were also inactive. These results are in agreement with our previous hypothesis that active compounds are characterized by R1 rings with moderate size substituents at the ortho and para positions.

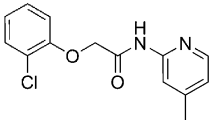
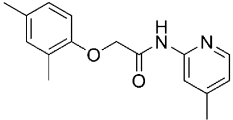
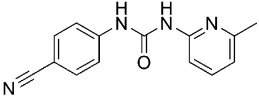
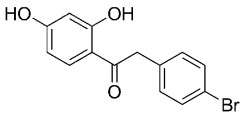
**Compound Optimization.** The seven hits (Table 2) all have a Michael acceptor functionality that is known to covalently bind to cysteines.<sup>43</sup> Therefore, we cannot exclude off-target binding to cysteines in proteins involved in the NF-

$\kappa B$  signaling pathway. Even though the two final compounds perform excellently in *in vivo* test systems, we decided to investigate the possibilities of placing a nonreactive linker between the two ring systems to reduce the risk of off-target effects.

We hand-picked 20 compounds from the top 25% of compounds identified in the primary *in vitro* screen (Figure 1, step 2a) that had a linker between the two rings consisting of two, three, or four atoms and no Michael acceptor functionality. These 20 compounds, structurally different to our previous set of compounds, were tested in the luciferase NF- $\kappa B$  cell-based assay. Ten compounds showed more than 25% inhibition at 10  $\mu M$ , and of those ten, four showed a dose-dependent response with an  $IC_{50}$  value in the range of 3–10  $\mu M$  (Table 6 and Figure 1, step 2b). These four compounds are characterized by ortho or para substitutions with groups like Cl, CH<sub>3</sub>, CN, or OH in ring R1 or groups like CH<sub>3</sub> or Br in ring R2. They have a range of different linkers, comprising two, three, or four atoms. The only common factor in the linkers is the C=O group. These four compounds were tested for direct binding to the C-domain of TRAF6. Compound 9078886 showed poor solubility at high concentrations and was removed from the experiment. Compounds 6576379 and 7113606 bind weakly (in the mM



Table 6. IC<sub>50</sub> Values ( $\mu$ M) of Compounds without a Michael Acceptor in the Linker

Compound #	ChemBridge ID	MW (kDa)	IC <sub>50</sub> ( $\mu$ M)	Structure
1	6576379	276.7	3.1	
2	5843084	270.3	8.0	
3	9078886	252.3	2.4	
4	7113606	307.1	9.3	

range) to the TRAF6 C-domain, whereas compound 5843084 has a  $K_d$  value of 52  $\mu$ M.

This preliminary round of modifications suggests that the potentially reactive linker can be replaced by a nonreactive linker while preserving the inhibitory activity of the compounds and argues against the covalent binding of cysteines as a sole explanation of the activities observed *in vitro* and *in vivo*.

**In Vivo Models.** The CD40 pathway plays a pivotal role in the NF- $\kappa$ B signaling that leads to inflammatory responses. Previously, we showed that compound 6877002 inhibits the NF- $\kappa$ B cell-based assay and reduced diet-induced insulin resistance.<sup>11</sup> Here, we show how we verified the inhibitory activity of the seven hits, including compound 6877002 (Table 1) in an *in vivo* model for acute inflammation, i.e., during peritonitis. We explain why we chose this compound for the other *in vivo* model, even though it did not show the best IC<sub>50</sub> values in the cell-based assay. The CD40 signaling plays a pivotal role in the innate immune response to polymicrobial sepsis.<sup>44</sup> Therefore, we show the effect of compound 6877002 and 6860766 in the treatment of sepsis.

**Peritonitis.** Inflammation of the peritoneum, peritonitis, is a model of acute inflammation. To assess the influence of our compounds on acute inflammation (Figure 1, step 4), we used a thioglycolate-induced peritonitis mouse model with the seven compounds listed in Table 2. Treatment for 1 week with each compound induced an anti-inflammatory peritoneal monocyte profile with an increased anti-inflammatory/pro-inflammatory monocyte ratio (Ly6C<sup>low</sup>/Ly6C<sup>high</sup>) that reduced inflammation ( $n = 6-8$  per group) (Figure 5). Data are presented as mean  $\pm$  SEM. Data were analyzed with a Student's two-tailed  $t$  test. Differences between compounds and vehicle groups were considered significant if  $p$ -value  $< 0.05$ . Financial constraints restricted testing of compounds in the further *in vivo* test to only two compounds. We selected two compounds (6872674 and 6877002) that had the best observed efficacy in the peritonitis model. Unfortunately, compound 6872674 showed significant precipitation at high concentrations (required to limit the volume of injected compound), which had not been

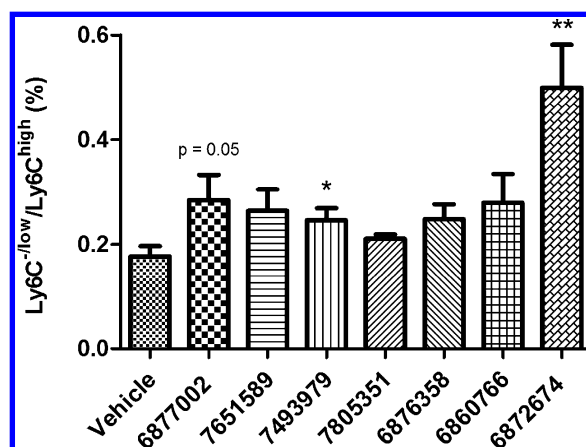
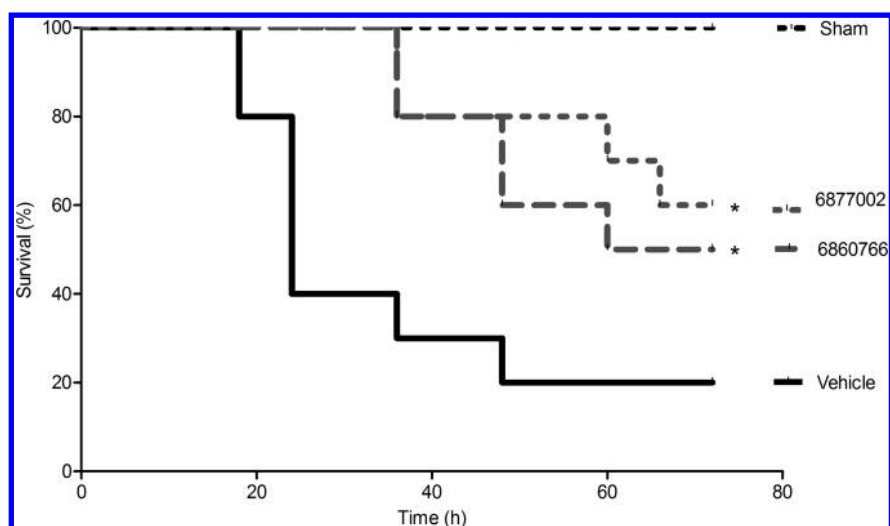


Figure 5. Increase of Ly6C<sup>low</sup>/Ly6C<sup>high</sup> monocytes ratio in the peritonitis model ( $n = 6-8$  per group).  $p$ -value  $< 0.05$  is indicated by \*.  $p$ -value  $< 0.01$  is indicated by \*\*.

observed in the earlier experiments. As a result, this compound had to be excluded from further analyses and was replaced by the next best compound (6860766).

**Sepsis.** Polymicrobial sepsis, as a model for intensive systemic inflammation, was induced in C57Bl6 mice by cecal ligation and puncture (CLP). After the CLP procedure, mice were treated with compound 6877002 or 6860766 (10  $\mu$ M/kg at  $t = 0$  h and  $t = 12$  h.). Survival rates were increased by 150% (6877002) and 200% (6860766) (Figure 6) showing that the compounds are protective against death from sepsis. Furthermore, this experiment showed that treatment with our inhibitors did not compromise systemic immunity.

Statistical significance of survival curves was determined using the log-rank (Mantel-Cox) and Gehan-Breslow-Wilcoxon test. Differences between compounds and vehicle groups with  $p$ -values  $< 0.05$  were considered significant.



**Figure 6.** Compound treatment improved the survival of mice subjected to sepsis. Compound 6877002-treated and compound 6860766-treated mice subjected to cecal ligation and puncture exhibited increased survival rates, suggesting that the compounds did not compromise systemic immunity during polymicrobial sepsis ( $n = 10$  per group). \*,  $p < 0.05$  (vehicle vs 6877002 or 6860766).

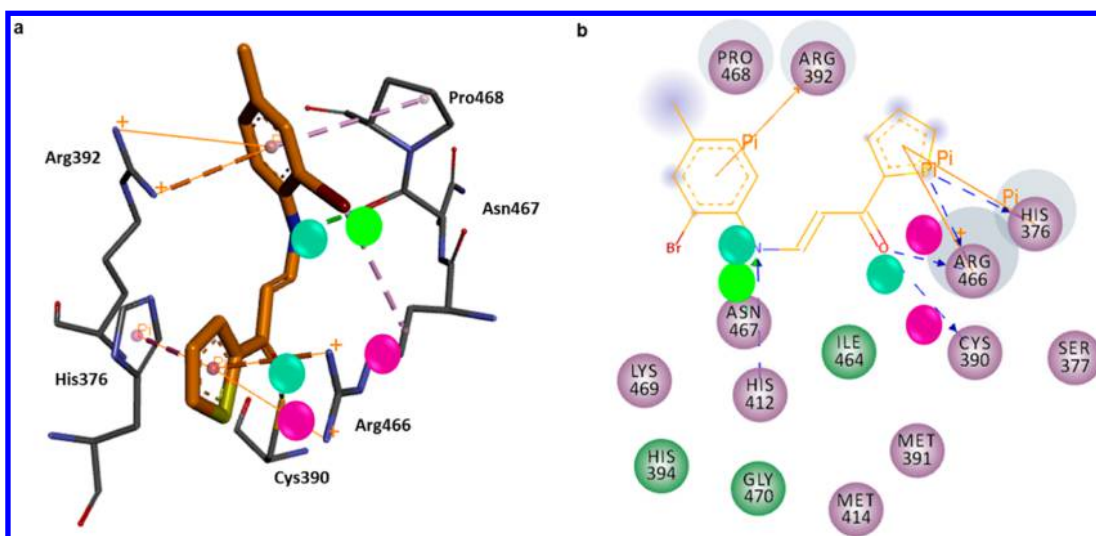


**Figure 7.** Predicted binding site with pharmacophore features: hydrophobic contacts (magenta ball), aromatic interactions (cyan ball), and H-bond acceptor (green ball). Further lines and colors as in Figure 4.

## DISCUSSION

Drug development has mainly been a trial and error process with some of its greatest discoveries based on serendipity and clinical observations.<sup>45</sup> The introduction of X-ray crystallography and computer power in the drug design process led to a paradigm shift from empirical to structure-based rational design.<sup>46</sup> More recently, we have seen some success stories in the form of marketed drugs designed mainly via an *in silico* approach.<sup>47,48</sup> Here, we present the rational design of an inhibitor validated through *in vivo* models. Despite the fact that we have identified potential lead compounds for CD40–TRAF6 interaction that are safe and efficacious in animal models, there is still a long way to go before we have a drug that can be administered routinely to patients. Further tests are essential, including ADME-tox studies, pharmacokinetics, and long-term safety studies that are outside the scope of the present work. However, the relative ease with which we have achieved our results show that VLS approaches in combination

with *in vitro* and *in vivo* screening like the one shown in Figure 1 have great potential.

Our lead compounds have confirmed efficacy in a diet-induced obesity mouse model. Treatment with one of our lead compounds improved insulin sensitivity, reduced adipose tissue inflammation, and decreased hepatosteatosis. These compounds are therefore considered a good starting point for the design of a treatment for obesity-associated insulin resistance.<sup>11</sup> The most active compounds do, however, contain a common linker that contains Michael acceptor functionality, which is known to include reactivity that can covalently bind to cysteines.<sup>43</sup> Even though the Michael acceptor is considered to be a PAIN (pan assay interference)<sup>49</sup> substructure and the presence of this functional group is generally considered drawback,<sup>50</sup> it has shown to be successful in kinase inhibitors that reached clinical phase III in breast cancer treatment.<sup>51</sup> In the optimization process, we found that compound 5843084, similar to our lead compounds, has a linker of four atoms long but lacks a Michael acceptor. This compound has an  $IC_{50}$  value

of 8  $\mu\text{M}$  in the NF- $\kappa\text{B}$  luciferase cell-based assay and in SPR showed binding to the C-domain of TRAF6 with a  $K_d$  value of 52  $\mu\text{M}$ . This preliminary study made clear that the linker that contains the Michael acceptor can easily be replaced without loss of *in vitro* activity.

The NMR spectra for the compounds with a Michael acceptor shown in Table 2 revealed that these compounds exist as *cis* and *trans* tautomers. On the basis of our *in silico* docking studies, we predicted that our compounds will bind as *trans* stereoisomers.  $K_d$  values from the Biacore studies were higher than expected from *in vitro* assays. This inconsistency may result from the fact that we did not measure homogeneous compounds but a mix of (*trans*) binders and (*cis*) nonbinders. This problem was one of the reasons for the 2D similarity search for binders without a Michael acceptor.

We also observed systematic differences in  $\text{IC}_{50}$  values between the two types of *in vitro* assays that were used to assess the *in vitro* activity of compounds in this study.  $\text{IC}_{50}$  values from different assays are generally not fully reproducible, as they depend on many different parameters and may not be comparable.<sup>52</sup> Apparent inconsistencies may well be due to the different origins of the cells used. The LPS-induced assay was performed in the mouse RAW 264.7 cell lines, whereas the CD40-induced assay used the mouse primary cells of BM-derived macrophages.

Even though our compounds were designed to bind to the TRAF6 protein, we cannot at this stage of project fully exclude off-target effects. To address potential off-target effects, we used the KRIPO software for off-target prediction. The pharmacophore used by KRIPO in this query consisted of five features: a hydrogen bond acceptor from the backbone oxygen from Asn467, stacking interactions from His376 and His412, and hydrophobic contacts from Cys390 (SH group in the side chain) and Arg466 ( $\text{CH}_2$  groups in the side chain) (Figure 7).

We obtained a hit list with 133 targets that share a similar pocket or subpocket with TRAF6. Eleven predicted off-targets share a full binding pocket with TRAF6 (Table 7). The other

**Table 7. Hit List with Potential Off-Targets as Identified by KRIPO.<sup>31</sup>**

target	name	PDB ID
1	amine oxidase	2XFN
2	dimethylsulfoniopropionate demethylase	3TFJ
3	$\alpha$ -N-acetylgalactosaminidase	2IXA
4	nitric oxide synthase, endothelial	1DM6
5	serine/threonine-protein kinase	4LKM
6	SOS ribosomal protein L1	2HW8
7	xylose isomerase	1O1H
8	orotidine 5'-phosphate decarboxylase	3N2M
9	proteorhodopsin	4JQ6
10	NAD(P)H flavin oxidoreductase	4BSN
11	gramicidin A	1AV2

122 off-targets only share a subpocket with TRAF6. These are listed in the Supporting Information. None of these targets is known to be involved in the NF- $\kappa\text{B}$  signaling pathway. For the 11 off-targets that share a full binding pocket with TRAF6, only the  $\alpha$ -N-acetylgalactosaminidase binding site is located at the enzyme's active site. The rest of the predicted binding sites are binding pockets located away from the main active site.

Off-target prediction with KRIPO resulted in relatively few pockets for TRAF6 compared to other KRIPO searches,<sup>31</sup>

suggesting that the binding pocket of TRAF6 is rather unique among the binding sites of protein–ligand complexes deposited in the PDB. There are more targets within the NF- $\kappa\text{B}$  signaling pathway that are used for structure-based design of anti-inflammatory drugs. The main one is IKK- $\beta$ .<sup>53</sup> The KRIPO search did not reveal IKK- $\beta$  as an off-target for TRAF6 ligands. In addition, docking of the seven hits with Flexy did not show any productive poses for this target. However, as KRIPO requires ligands to be present as heterogroups in the PDB files in its database, we cannot exclude that peptide-binding off-targets such as E3 ubiquitin ligases, PDB ID: 2FOJ,<sup>54</sup> exist.

TRAF6 mediates signaling from members of the TNF receptor superfamily such as the CD40 receptor and from members of the Toll/IL-1 family such as the Toll-like receptor 4 (TLR4). It plays different roles in these two signaling pathways. In CD40 signaling, the C-domain of TRAF6 creates a protein–protein interaction complex with the intracellular part of the CD40 receptor, which results in activation of the NF- $\kappa\text{B}$  signaling pathway. The RING-domain of TRAF6 serves as an E3 ubiquitin ligase and activates I $\kappa$ B kinase (IKK), contributing to TLR4 signaling in the NF- $\kappa\text{B}$  pathway.<sup>55</sup> Thus, inhibition of post-translational modification such as ubiquitination can also inhibit inflammation.<sup>56</sup> Such polypharmacological advantages, though, are beyond the scope of this article.

CD40 shows structural differences between binding to the C-domain of TRAF6 and TRAF 2, 3, and 5.<sup>12</sup> We hypothesized that structural differences between the TRAF6 and other TRAF proteins will facilitate the design of CD40–TRAF6 specific compounds. SPR experiments confirmed that compounds 6877002 and 6860766 bind to the C-domain of TRAF6 with  $K_d$  values of 97<sup>11</sup> and 59  $\mu\text{M}$  (Figure 1, step 4a), respectively. However, when the direct binding of these two compounds to the C-domain of TRAF 1, 2, 3, and 6 was investigated via SPR, both compounds appeared to bind to the C-domain of all these TRAF proteins in the  $\mu\text{M}$  range (30–144  $\mu\text{M}$ ) (Table 8).

**Table 8. SPR Direct Binding Experiment with TRAF 1, 2, 3, and 6 Proteins**

target	6877002 $K_d$ [ $\mu\text{M}$ ]	6860766 $K_d$ [ $\mu\text{M}$ ]
TRAF1	142	51
TRAF2	144	30
TRAF3	99	37
TRAF6	141	59

Because all the TRAF proteins share similar structures, this finding is not unexpected in a nonbiological setting, where the interactions of the TRAF proteins with their different receptors (e.g., CD40, TLR4, CD27, Ox40L, and RANKL), and the conformational changes that occur in real life are disregarded. Although we cannot fully rule out interference of our compounds with other receptor–TRAF interactions, we could confirm functional specificity for the CD40–TRAF6 and not the CD40–TRAF 2, 3, and 5 pathway, *in vitro* and *in vivo*.<sup>11</sup>

Previously, it has been shown that blocking the complete CD40 pathway leads to severe side effects.<sup>9</sup> Therefore, our goal was to design specific compounds targeted at TRAF6 to block the TRAF6–CD40 interaction, while at the same time maintaining signaling of the CD40 pathway via other TRAFs. To verify possible toxicity, the RAW cells were incubated with compounds at 10  $\mu\text{M}$ . Compounds did not induce any changes in cell viability. Further, compounds were administered for



seven days in the mice at 10  $\mu\text{M}/\text{kg}$ . This treatment did not result in micro- or macroscopic abnormalities of greater than 13 organs analyzed nor did it influence absolute or relative peripheral blood leukocyte counts. Histological analysis of vital organs showed no toxic, immunosuppressive, or thromboembolic side effects of compound treatment. Therefore, seven compounds did not show toxicity in an *in vitro* viability assay or in *in vivo* treatment. In addition, our compounds do not bind with affinities that would be high enough to completely block CD40 signaling. Like CD40–TRAF6 interactions, they bind in the  $\mu\text{M}$  range. This suggests that our relatively weak binding lead compounds can inhibit CD40–TRAF6 interactions with high efficacy because they have the capacity to compete with a natural partner that binds in the same  $\mu\text{M}$  range.<sup>12</sup>

We present an *in silico* screening pipeline to discover hit molecules that inhibit CD40 signaling. Both *in vitro*, and *in vivo* experiments showed that our compounds show efficacy without side effects in mouse models for obesity associated insulin resistance,<sup>11</sup> peritonitis, and sepsis. We showed that the compounds can be optimized and have potential for the further development of treatment for (chronic) inflammatory diseases.

## ■ ASSOCIATED CONTENT

### ■ Supporting Information

Information as mentioned in the text. This material is available free of charge via the Internet at <http://pubs.acs.org>.

## ■ AUTHOR INFORMATION

### Corresponding Author

\*Tel.: +31 43 3881688. Fax: +31 43 3884159. E-mail: g.nicolaes@maastrichtuniversity.nl

### Author Contributions

B. Zarzycka and T. Seijkens contributed equally to this work.

### Author Contributions

E. Lutgens, G. Vriend, and G. A. F. Nicolaes contributed equally to this work.

### Notes

The authors declare no competing financial interest.

## ■ ACKNOWLEDGMENTS

This work was supported by the Humboldt Foundation [Sofja Kovalevskaja grant (to E.L.)], The Netherlands Organisation for Scientific Research [vici grant (to E.L.), a medium investment grant (to G.N.)], The Netherlands Heart Foundation [Dr. E. Dekker grant (to T.S.) and an established investigator grant (to E.L.)], the Rembrandt foundation (to E.L.), the Deutsche Forschungsgemeinschaft [SFB914, SFB 1054, and SFB1123 (to E.L. O.S. and C.W.)], the Cardiovascular Research Institute Maastricht (to G.N.), the European Union [Grant KBBE-2011-5 289350, AllBio, and EFRO (to G.V.)], the Transnational University Limburg (to G.N.), and Cytron II [FES0908 (to G.N. and T.H.)]. We thank Jan Kelder and Hugo Kubinyi (who persuaded us to go from Step 2 to Step 2a and 2b in our drug selection pipeline) for critical reading of the manuscript. We thank F. Albayrak for technical assistance.

## ■ ABBREVIATIONS

TNF, tumor necrosis factor; TRAF, TNF receptor-associated factor; JNK, C-Jun N-terminal kinase; MAP, p38 mitogen activated protein; ADME/tox, administration, delivery, metabolism, extraction, and toxicity; RMSD, root-mean-square

deviation; VLS, virtual ligand screening; FRED, fast rigid exhaustive docking; KRIPO, key representation of interaction in pockets; LPS, lipopolysaccharide; BM, bone marrow; RU, response units; PBST, phosphate-buffered saline with Triton X-100; PBS, phosphate-buffered saline; SPR, surface plasmon resonance;  $K_{\text{d}}$ s, equilibrium dissociation constants; CLP, cecal ligation and puncture; SAR, structure–activity relationship; PAIN, pan assay interference; RAW 264.7, mouse monocyte/macrophage cell line; GST, glutathione S-transferase

## ■ REFERENCES

- (1) Schönbeck, U.; Libby, P. The CD40/CD154 Receptor/ligand Dyad. *Cell. Mol. Life Sci.* **2001**, *58*, 4–43.
- (2) Arron, J. R.; Pewzner-Jung, Y.; Walsh, M. C.; Kobayashi, T.; Choi, Y. Regulation of the Subcellular Localization of Tumor Necrosis Factor Receptor-Associated Factor (TRAF)2 by TRAF1 Reveals Mechanisms of TRAF2 Signaling. *J. Exp. Med.* **2002**, *196*, 923–934.
- (3) Zapata, J. M. TNF-Receptor-Associated Factors as Targets for Drug Development. *Expert Opin. Ther. Targets* **2003**, *7*, 411–425.
- (4) Desideri, G.; Ferri, C. Effects of Obesity and Weight Loss on Soluble CD40L Levels. *JAMA, J. Am. Med. Assoc.* **2003**, *289*, 1781–1782.
- (5) Kuwana, M.; Nomura, S.; Fujimura, K.; Nagasawa, T.; Muto, Y.; Kurata, Y.; Tanaka, S.; Ikeda, Y. Effect of a Single Injection of Humanized Anti-CD154 Monoclonal Antibody on the Platelet-Specific Autoimmune Response in Patients with Immune Thrombocytopenic Purpura. *Blood* **2004**, *103*, 1229–1236.
- (6) Boumpas, D. T.; Furie, R.; Manzi, S.; Illei, G. G.; Wallace, D. J.; Balow, J. E.; Vaishnaw, A. BG9588 Lupus Nephritis Trial Group. A Short Course of BG9588 (anti-CD40 Ligand Antibody) Improves Serologic Activity and Decreases Hematuria in Patients with Proliferative Lupus Glomerulonephritis. *Arthritis Rheum.* **2003**, *48*, 719–727.
- (7) Davis, J. C.; Totoritis, M. C.; Rosenberg, J.; Sklenar, T. A.; Wofsy, D. Phase I Clinical Trial of a Monoclonal Antibody against CD40-Ligand (IDEC-131) in Patients with Systemic Lupus Erythematosus. *J. Rheumatol.* **2001**, *28*, 95–101.
- (8) Silvian, L. F.; Friedman, J. E.; Strauch, K.; Cachero, T. G.; Day, E. S.; Qian, F.; Cunningham, B.; Fung, A.; Sun, L.; Shipps, G. W.; Su, L.; Zheng, Z.; Kumaravel, G.; Whitty, A. Small Molecule Inhibition of the TNF Family Cytokine CD40 Ligand through a Subunit Fracture Mechanism. *ACS Chem. Biol.* **2011**, *6*, 636–647.
- (9) Kawai, T.; Andrews, D.; Colvin, R. B.; Sachs, D. H.; Cosimi, A. B. Thromboembolic Complications after Treatment with Monoclonal Antibody against CD40 Ligand. *Nat. Med.* **2000**, *6*, 114.
- (10) Lutgens, E.; Lievens, D.; Beckers, L.; Wijnands, E.; Soehnlein, O.; Zernecke, A.; Seijkens, T.; Engel, D.; Cleutjens, J.; Keller, A. M.; Naik, S. H.; Boon, L.; Oufella, H. A.; Mallat, Z.; Ahonen, C. L.; Noelle, R. J.; de Winther, M. P.; Daemen, M. J.; Biessen, E. A.; Weber, C. Deficient CD40–TRAF6 Signaling in Leukocytes Prevents Atherosclerosis by Skewing the Immune Response toward an Antiinflammatory Profile. *J. Exp. Med.* **2010**, *207*, 391–404.
- (11) Chatzigeorgiou, A.; Seijkens, T.; Zarzycka, B.; Engel, D.; Poggi, M.; van den Berg, S.; van den Berg, S.; Soehnlein, O.; Winkels, H.; Beckers, L.; Lievens, D.; Driessen, A.; Kusters, P.; Biessen, E.; Garcia-Martin, R.; Klotzsche-von Ameln, A.; Gijbels, M.; Noelle, R.; Boon, L.; Hackeng, T.; Schulte, K.-M.; Schulte, K.; Xu, A.; Vriend, G.; Nabuurs, S.; Chung, K.-J.; Willems van Dijk, K.; Rensen, P. C. N.; Gerdes, N.; de Winther, M.; Block, N. L.; Schally, A. V.; Weber, C.; Bornstein, S. R.; Nicolaes, G.; Chavakis, T.; Lutgens, E. Blocking CD40–TRAF6 Signaling Is a Therapeutic Target in Obesity-Associated Insulin Resistance. *Proc. Natl. Acad. Sci. U.S.A.* **2014**, *111*, 2686–2691.
- (12) Ye, H.; Arron, J. R.; Lamothe, B.; Cirilli, M.; Kobayashi, T.; Shevde, N. K.; Segal, D.; Dziveno, O. K.; Vologodskaya, M.; Yim, M.; Du, K.; Singh, S.; Pike, J. W.; Darnay, B. G.; Choi, Y.; Wu, H. Distinct Molecular Mechanism for Initiating TRAF6 Signalling. *Nature* **2002**, *418*, 443–447.



- (13) Bernstein, F. C.; Koetzle, T. F.; Williams, G. J.; Meyer, E. F.; Brice, M. D.; Rodgers, J. R.; Kennard, O.; Shimanouchi, T.; Tasumi, M. The Protein Data Bank: A Computer-Based Archival File for Macromolecular Structures. *J. Mol. Biol.* **1977**, *112*, 535–542.
- (14) Krieger, E.; Koraimann, G.; Vriend, G. Increasing the Precision of Comparative Models with YASARA NOVA—A Self-Parameterizing Force Field. *Proteins* **2002**, *47*, 393–402.
- (15) Hooft, R. W.; Sander, C.; Vriend, G. Positioning Hydrogen Atoms by Optimizing Hydrogen-Bond Networks in Protein Structures. *Proteins* **1996**, *26*, 363–376.
- (16) Vriend, G.; Sander, C. Detection of Common Three-Dimensional Substructures in Proteins. *Proteins* **1991**, *11*, 52–58.
- (17) Dunbrack, R. L.; Cohen, F. E. Bayesian Statistical Analysis of Protein Side-Chain Rotamer Preferences. *Protein Sci. Publ. Protein Soc.* **1997**, *6*, 1661–1681.
- (18) An, J.; Totrov, M.; Abagyan, R. Pocketome via Comprehensive Identification and Classification of Ligand Binding Envelopes. *Mol. Cell. Proteomics* **2005**, *4*, 752–761.
- (19) Laurie, A. T. R.; Jackson, R. M. Q-SiteFinder: An Energy-Based Method for the Prediction of Protein–Ligand Binding Sites. *Bioinformatics* **2005**, *21*, 1908–1916.
- (20) ChemBridge Corp. San Diego CA USA [www.chembridge.com](http://www.chembridge.com).
- (21) Lagorce, D.; Sperandio, O.; Galons, H.; Miteva, M. A.; Villoutreix, B. O. FAF-Drugs2: Free ADME/tox Filtering Tool To Assist Drug Discovery and Chemical Biology Projects. *BMC Bioinf.* **2008**, *9*, 396.
- (22) Rishton, G. M. Nonleadlikeness and Leadlikeness in Biochemical Screening. *Drug Discovery Today* **2003**, *8*, 86–96.
- (23) Miteva, M. A.; Violas, S.; Montes, M.; Gomez, D.; Tuffery, P.; Villoutreix, B. O. FAF-Drugs: Free ADME/tox Filtering of Compound Collections. *Nucleic Acids Res.* **2006**, *34*, W738–W744.
- (24) Hawkins, P. C. D.; Skillman, A. G.; Warren, G. L.; Ellingson, B. A.; Stahl, M. T. Conformer Generation with OMEGA: Algorithm and Validation Using High Quality Structures from the Protein Databank and Cambridge Structural Database. *J. Chem. Inf. Model.* **2010**, *50*, 572–584.
- (25) Miteva, M. A.; Lee, W. H.; Montes, M. O.; Villoutreix, B. O. Fast Structure-Based Virtual Ligand Screening Combining FRED, DOCK, and Surflex. *J. Med. Chem.* **2005**, *48*, 6012–6022.
- (26) Du, J.; Bleylevens, I. W. M.; Bitorina, A. V.; Wichapong, K.; Nicolaes, G. A. F. Optimization of Compound Ranking for Structure-Based Virtual Ligand Screening Using an Established FRED-Surflex Consensus Approach. *Chem. Biol. Drug Des.* **2014**, *83*, 37–51.
- (27) McGann, M. FRED Pose Prediction and Virtual Screening Accuracy. *J. Chem. Inf. Model.* **2011**, *51*, 578–596.
- (28) ChemBridge Corp. [www.hit2lead.com](http://www.hit2lead.com) (accessed January 2015).
- (29) Jain, A. N. Surflex: Fully Automatic Flexible Molecular Docking Using a Molecular Similarity-Based Search Engine. *J. Med. Chem.* **2003**, *46*, 499–511.
- (30) Tanimoto, T. T. IBM Internal Report, November 17, 1957.
- (31) Wood, D. J.; de Vlieg, J.; Wagener, M.; Ritschel, T. Pharmacophore Fingerprint-Based Approach to Binding Site Sub-pocket Similarity and Its Application to Bioisostere Replacement. *J. Chem. Inf. Model.* **2012**, *52*, 2031–2043.
- (32) Nabuurs, S. B.; Wagener, M.; de Vlieg, J. A Flexible Approach to Induced Fit Docking. *J. Med. Chem.* **2007**, *50*, 6507–6518.
- (33) Carlsen, H.; Moskaug, J. Ø.; Fromm, S. H.; Blomhoff, R. In Vivo Imaging of NF-Kappa B Activity. *J. Immunol. Baltim. Md 1950* **2002**, *168*, 1441–1446.
- (34) Shkoda, A.; Town, J. A.; Griese, J.; Romio, M.; Sarioglu, H.; Knöfel, T.; Giehler, F.; Kieser, A. The Germinal Center Kinase TNK1 Is Required for Canonical NF- $\kappa$ B and JNK Signaling in B-Cells by the EBV Oncoprotein LMP1 and the CD40 Receptor. *PLoS Biol.* **2012**, *10*, e1001376.
- (35) De Jong, S. J.; Albrecht, J.-C.; Giehler, F.; Kieser, A.; Sticht, H.; Biesinger, B. Noncanonical NF- $\kappa$ B Activation by the Oncoprotein Tio Occurs through a Nonconserved TRAF3-Binding Motif. *Sci. Signal* **2013**, *6*, ra27.
- (36) BIAcore AB. *Kinetics and Affinity Analysis Using BIA - Level 1*, 1997.
- (37) Grommes, J.; Vijayan, S.; Drechsler, M.; Hartwig, H.; Mörgelin, M.; Dembinski, R.; Jacobs, M.; Koeppl, T. A.; Binnebösel, M.; Weber, C.; Soehnlein, O. Simvastatin Reduces Endotoxin-Induced Acute Lung Injury by Decreasing Neutrophil Recruitment and Radical Formation. *PLoS One* **2012**, *7*, e38917.
- (38) Seeliger, D.; de Groot, B. L. Conformational Transitions upon Ligand Binding: Holo-Structure Prediction from Apo Conformations. *PLoS Comput. Biol.* **2010**, *6*, e1000634.
- (39) Sperandio, O.; Miteva, M. A.; Segers, K.; Nicolaes, G. A. F.; Villoutreix, B. O. Screening Outside the Catalytic Site: Inhibition of Macromolecular Inter-Actions Through Structure-Based Virtual Ligand Screening Experiments. *Open Biochem. J.* **2008**, *2*, 29–37.
- (40) Segers, K.; Sperandio, O.; Sack, M.; Fischer, R.; Miteva, M. A.; Rosing, J.; Nicolaes, G. A. F.; Villoutreix, B. O. Design of Protein–membrane Interaction Inhibitors by Virtual Ligand Screening, Proof of Concept with the C2 Domain of Factor V. *Proc. Natl. Acad. Sci. U.S.A.* **2007**, *104*, 12697–12702.
- (41) Charifson, P. S.; Corkery, J. J.; Murcko, M. A.; Walters, W. P. Consensus Scoring: A Method for Obtaining Improved Hit Rates from Docking Databases of Three-Dimensional Structures into Proteins. *J. Med. Chem.* **1999**, *42*, 5100–5109.
- (42) Life Chemicals. <http://www.lifechemicals.com/> (accessed August 4, 2014).
- (43) Bergmann, E. D.; Ginsburg, D.; Pappo, R. The Michael Reaction. In *Organic Reactions*; John Wiley & Sons, Inc.: New York, 2004.
- (44) Gold, J. A.; Parsey, M.; Hoshino, Y.; Hoshino, S.; Nolan, A.; Yee, H.; Tse, D. B.; Weiden, M. D. CD40 Contributes to Lethality in Acute Sepsis: In Vivo Role for CD40 in Innate Immunity. *Infect. Immun.* **2003**, *71*, 3521–3528.
- (45) Ban, T. A. The Role of Serendipity in Drug Discovery. *Dialogues Clin. Neurosci.* **2006**, *8*, 335–344.
- (46) Hol, W. G. J. Protein Crystallography and Computer Graphics—Toward Rational Drug Design. *Angew. Chem., Int. Ed. Engl.* **1986**, *25*, 767–778.
- (47) Villoutreix, B. O.; Eudes, R.; Miteva, M. A. Structure-Based Virtual Ligand Screening: Recent Success Stories. *Comb. Chem. High Throughput Screening* **2009**, *12*, 1000–1016.
- (48) Seifert, M. H. J.; Lang, M. Essential Factors for Successful Virtual Screening. *Mini-Rev. Med. Chem.* **2008**, *8*, 63–72.
- (49) Baell, J. B.; Holloway, G. A. New Substructure Filters for Removal of Pan Assay Interference Compounds (PAINS) from Screening Libraries and for Their Exclusion in Bioassays. *J. Med. Chem.* **2010**, *53*, 2719–2740.
- (50) Park, B. K.; Boobis, A.; Clarke, S.; Goldring, C. E. P.; Jones, D.; Kenna, J. G.; Lambert, C.; Lavery, H. G.; Naisbitt, D. J.; Nelson, S.; Nicoll-Griffith, D. A.; Obach, R. S.; Routledge, P.; Smith, D. A.; Tweedie, D. J.; Vermeulen, N.; Williams, D. P.; Wilson, I. D.; Baillie, T. A. Managing the Challenge of Chemically Reactive Metabolites in Drug Development. *Nat. Rev. Drug Discovery* **2011**, *10*, 292–306.
- (51) Solca, F.; Dahl, G.; Zoephel, A.; Bader, G.; Sanderson, M.; Klein, C.; Kraemer, O.; Himmelsbach, F.; Haaksma, E.; Adolf, G. R. Target Binding Properties and Cellular Activity of Afatinib (BIBW 2992), an Irreversible ErbB Family Blocker. *J. Pharmacol. Exp. Ther.* **2012**, *343*, 342–350.
- (52) Kalliokoski, T.; Kramer, C.; Vulpetti, A.; Gedeck, P. Comparability of Mixed IC<sub>50</sub> Data – A Statistical Analysis. *PLoS One* **2013**, *8*, e61007.
- (53) Karin, M.; Yamamoto, Y.; Wang, Q. M. The IKK NF-Kappa B System: A Treasure Trove for Drug Development. *Nat. Rev. Drug Discovery* **2004**, *3*, 17–26.
- (54) Sheng, Y.; Saridakis, V.; Sarkari, F.; Duan, S.; Wu, T.; Arrowsmith, C. H.; Frappier, L. Molecular Recognition of p53 and MDM2 by USP7/HAUSP. *Nat. Struct. Mol. Biol.* **2006**, *13*, 285–291.
- (55) Xie, P. TRAF Molecules in Cell Signaling and in Human Diseases. *J. Mol. Signal.* **2013**, *8*, 7.

(56) Guédât, P.; Colland, F. Patented Small Molecule Inhibitors in the Ubiquitin Proteasome System. *BMC Biochem.* **2007**, 8 (Suppl 1), S14.

(57) Wu, H.; Arron, J. R. TRAF6, a Molecular Bridge Spanning Adaptive Immunity, Innate Immunity and Osteoimmunology. *BioEssays* **2003**, 25, 1096–1105.